Ni_3S_2/M_xS_y–NiCo LDH (M = Cu, Fe, V, Ce, Bi) heterostructure nanosheet arrays on Ni foam as high-efficiency electrocatalyst boosting for electrocatalytic overall water splitting and urea splitting

Chenyi Zhang[a], Xiaoqiang Du[a*], Xiaoshuang Zhang[b] and Yanhong Wang[a]

[a]School of Chemical Engineering and Technology, North University of China, Xueyuan road 3, Taiyuan 030051, People's Republic of China. E-mail: duxq16@nuc.edu.cn

[b]School of Science, North University of China, Xueyuan road 3, Taiyuan 030051, People's Republic of China.

DFT computation details:

The DFT calculations were performed using the Cambridge Sequential Total Energy Package (CASTEP) with the plane-wave pseudo-potential method. The geometrical structures of the (003) plane of $Ni(OH)_2$, the (003) plane of Ni_3S_2 and the (002) plane of CuS was optimized by the generalized gradient approximation (GGA) methods. The Revised Perdew-Burke-Ernzerh of (RPBE) functional was used to treat the electron exchange correlation interactions. A Monkhorst Pack grid k-points of 5*5*1 of Co-$Ni(OH)_2$, CuS and Ni_3S_2, a plane-wave basis set cut-off energy of 500 eV were used for integration of the Brillouin zone. The structures were optimized for energy and force convergence set at 0.05 eV/A and 2.0×10^{-5} eV, respectively.

Experiment section

Materials Characterization

The XRD patterns were reported from a Philips 1130 X-ray diffractometer (40 kV, 30 mA, Cu KR radiation, λ=1.5418 Å). The morphology of the Ni_3S_2/CuS-NiCo LDH/NF, Ni_3S_2/FeS-NiCo LDH/NF, Ni_3S_2/VS-NiCo LDH/NF, Ni_3S_2/CeS-NiCo LDH/NF and Ni_3S_2/Bi_2S_3-NiCo LDH/NF material is characterized by SEM images (Hitachi S-4800). TEM and HRTEM images were performed on a JEM-2100 with an accelerating voltage of 200 kV. The chemical composition and elemental states were analyzed by X-ray photoelectron spectroscopy (XPS, Axis Ultra DLD) using 60 W monochromated Mg Kα radiations as the exciting source.

Electrochemical measurements

Electrocatalytic tests were done with a CHI 760E electrochemical workstation (CH Instruments, Inc., Shanghai) in a typical three-electrode device. The resulting self-supported Ni_3S_2/CuS-NiCo LDH/NF, Ni_3S_2/FeS-NiCo LDH/NF, Ni_3S_2/VS-NiCo LDH/NF, Ni_3S_2/CeS-NiCo LDH/NF and Ni_3S_2/Bi_2S_3-NiCo LDH/NF electrodes were directly utilized as working electrode, a graphite rod and Ag/AgCl as counter electrode and reference electrode, respectively. All measured potentials in this work were calibrated to RHE according to the following equation: E (RHE) = E (Ag/AgCl) + (0.197 + 0.059* pH). Linear sweep voltammetry polarization curves were performed in 1 M KOH solution at a scan rate of 5 mV s^{-1}. Electrochemical impedance spectra (EIS) were collected at a frequency between 100 kHz and 0.01 Hz. In water splitting tests, all results were revised by ohmic potentials drop (iR) correction. The electrolyte for OER measurements was 1 M KOH, whereas the UOR performances were evaluated in 1 M KOH with 0.5 M urea. The stability measurements were recorded by chronopotentiometry measurements.

The faradaic efficiency (FE) was calculated by comparing the experimentally measured gas volume with the theoretically calculated value by a classic gas chromatographic method.

Through the collected gas amounts compared with the theoretically calculated values, the FE has been calculated as 88% by the follow equations of (1):

$$FE = (n \times z \times F)/I \times t \qquad (1)$$

in which, n is the actual moles number of products (the value can be evaluated by the collected gas amounts), z is the reaction electron number (the value is 6 as for 1 mol N_2), F is Faraday constant (96485 C mol^{-1}), I is the current (A), t is the test time (s)."

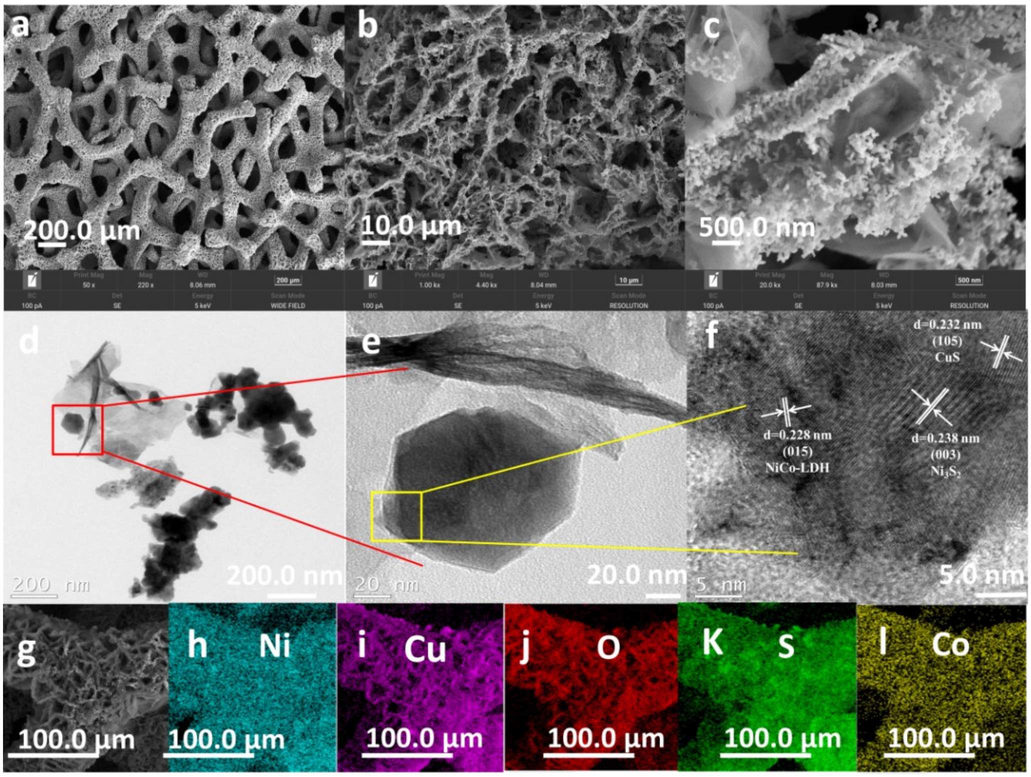

Fig. S1 (a–c) Typical SEM images of the Ni_3S_2/CuS-NiCo LDH on Ni foam; (d) TEM image of the Ni_3S_2/CuS-NiCo LDH/NF; (e) enlarged TEM image of the Ni_3S_2/CuS-NiCo LDH/NF; (f) HRTEM image of the Ni_3S_2/CuS-NiCo LDH/NF nanosheets; (g-k) EDX element mapping of Ni, Cu, O, S, and Co.

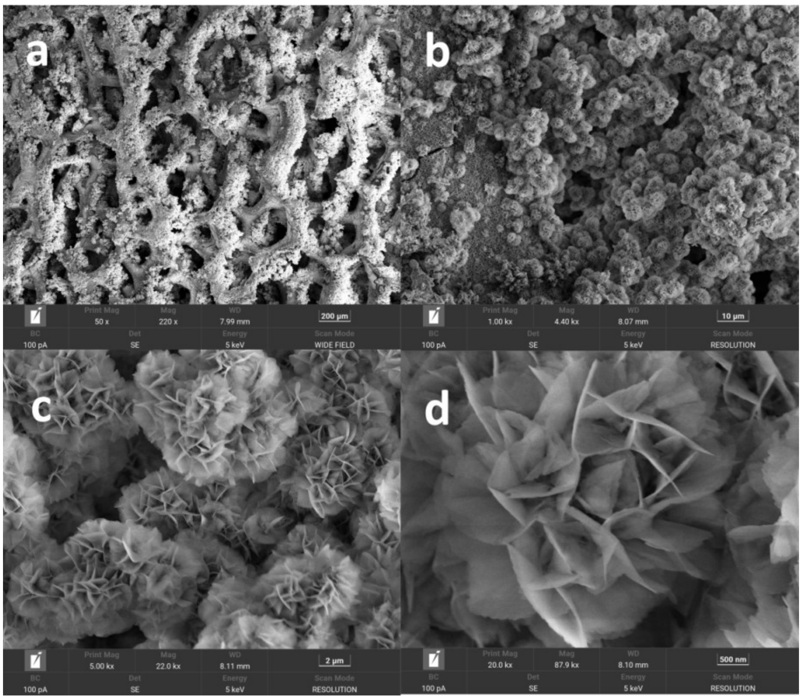

Fig. S2 (a–d) Typical SEM images of the Ni_3S_2/FeS-NiCo LDH on Ni foam.

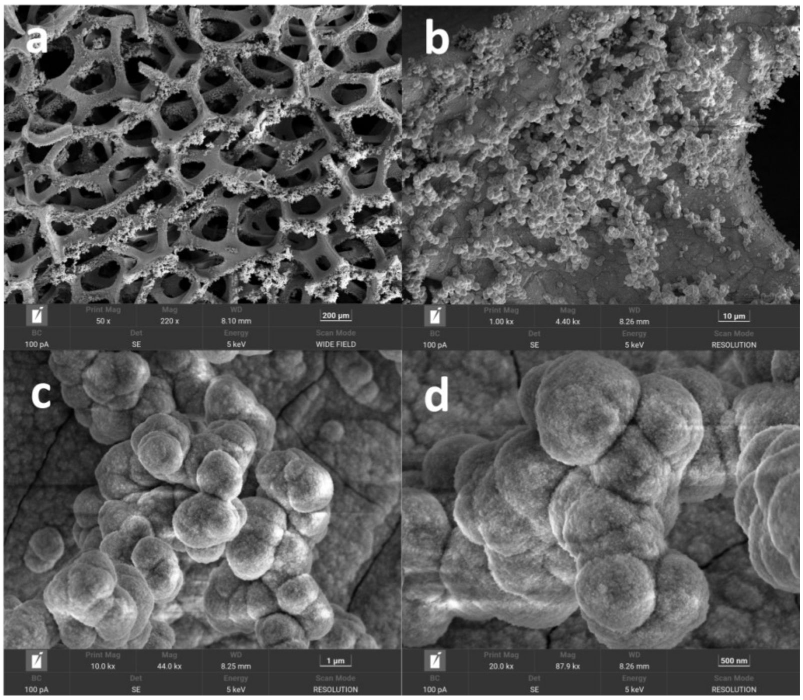

Fig. S3 (a–d) Typical SEM images of the Ni_3S_2/VS-NiCo LDH on Ni foam.

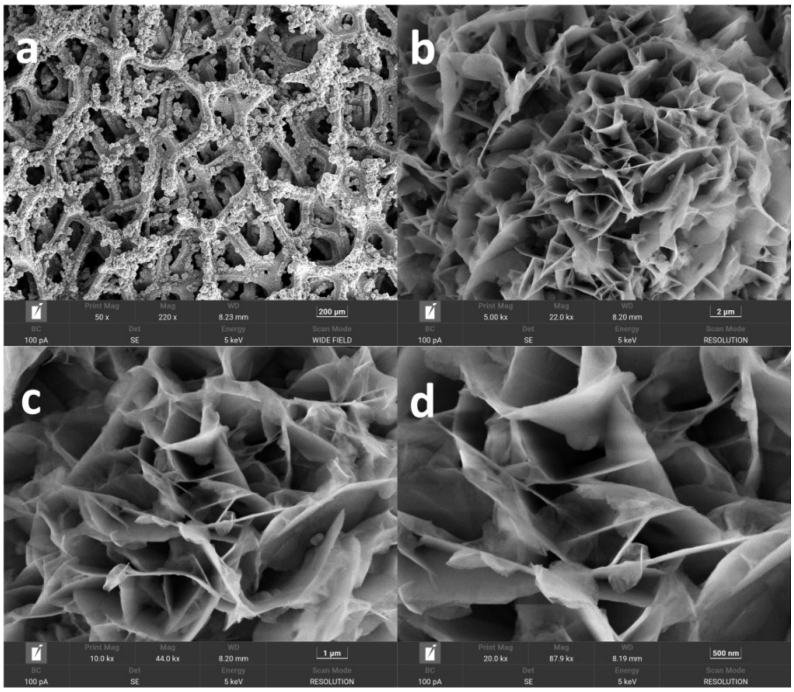

Fig. S4 (a–d) Typical SEM images of the Ni_3S_2/CeS-NiCo LDH on Ni foam.

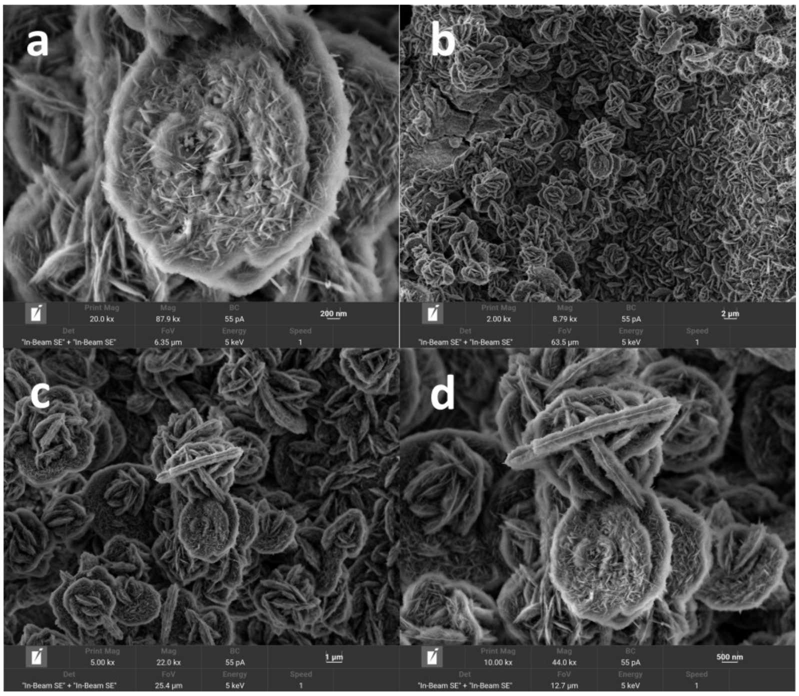

Fig. S5 (a–d) Typical SEM images of the NiCo LDH on Ni foam.

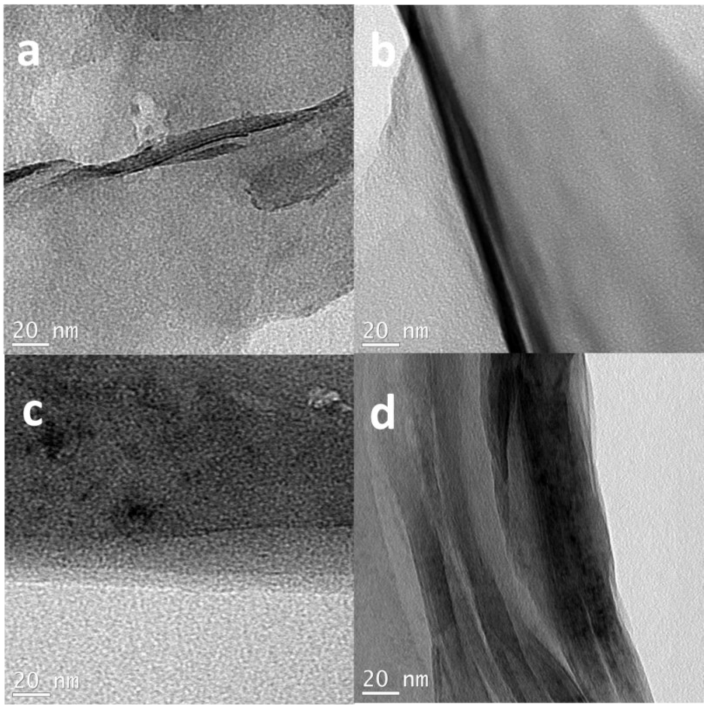

Fig. S6 (a–d) enlarged TEM image of the NS/BS-NC LDH.

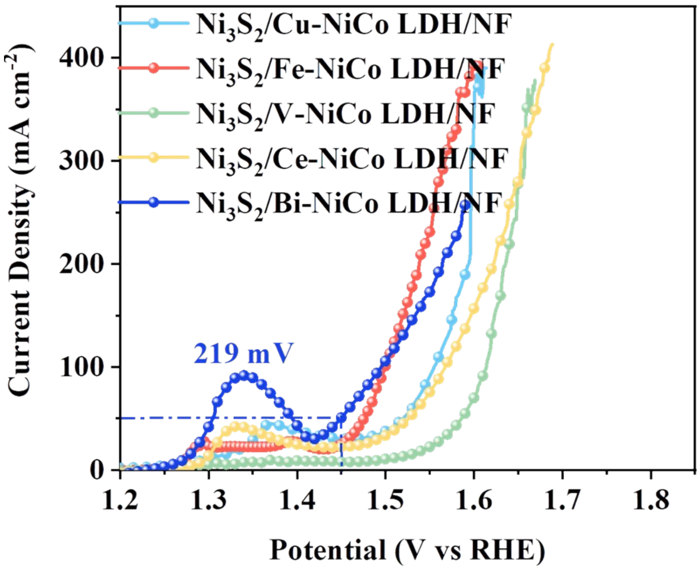

Fig. S7 LSV of Ni_3S_2/M_xS_y-NiCo LDH/NF with a scan rate of 5 mV/s in a 1 M KOH solution.

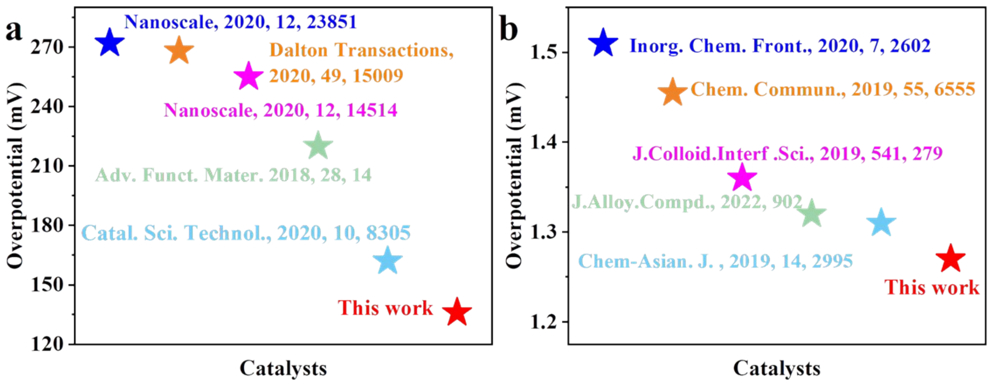

Fig. S8 Comparison of overpotentials of (a) OER [1-5] and (b) UOR [6-10].

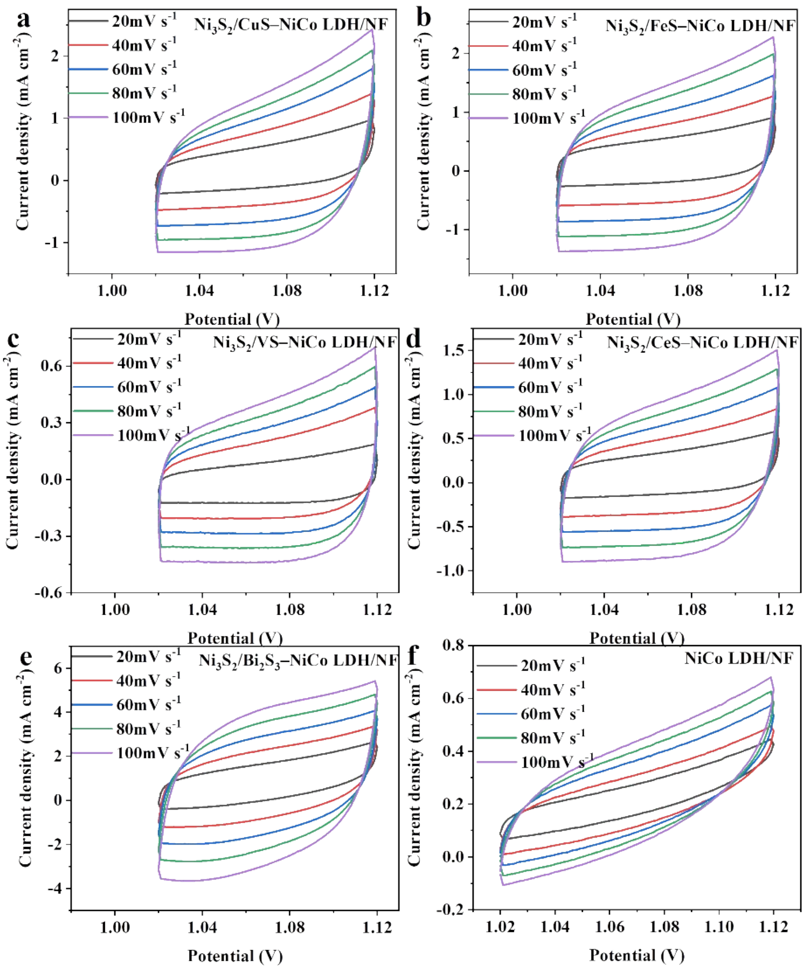

Fig. S9 In 1.0 M KOH, OER cyclic voltammograms of a) Ni_3S_2/CuS-NiCo LDH/NF, b) Ni_3S_2/FeS-NiCo LDH/NF, c) Ni_3S_2/VS-NiCo LDH/NF d) Ni_3S_2/CeS-NiCo LDH/NF and e) Ni_3S_2/Bi_2S_3-NiCo LDH/NF at the different scan rates varying from 20 to 100 mV·s^{-1}.

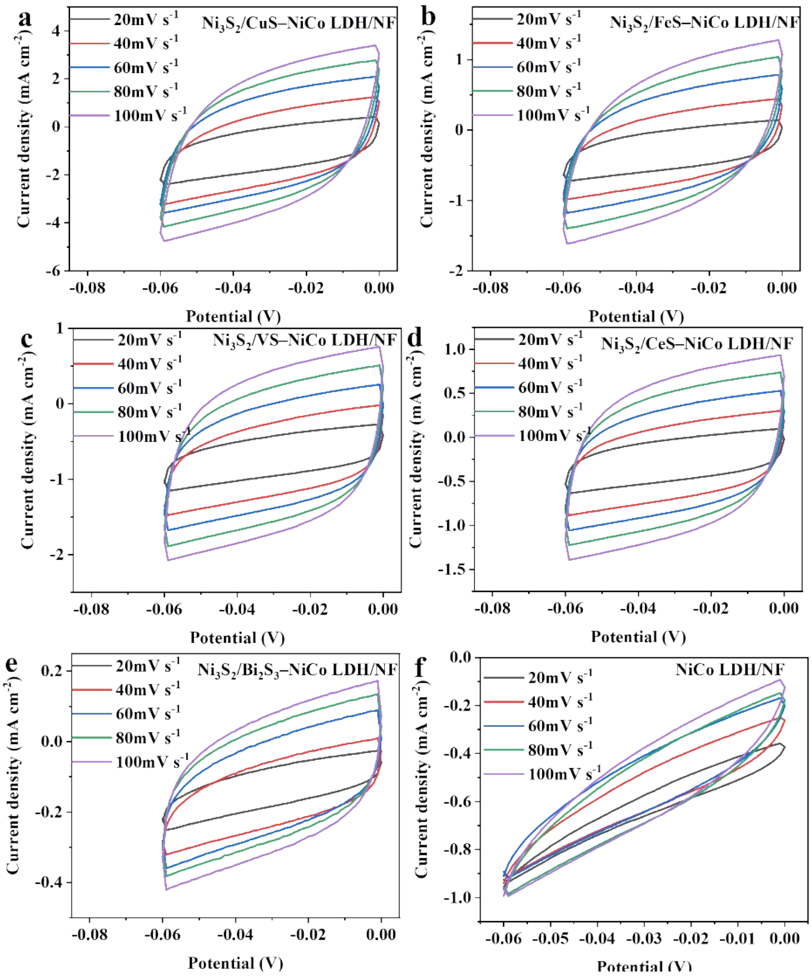

Fig. S10 In 1.0 M KOH, HER cyclic voltammograms of a) Ni_3S_2/CuS-NiCo LDH/NF, b) Ni_3S_2/FeS-NiCo LDH/NF, c) Ni_3S_2/VS-NiCo LDH/NF d) Ni_3S_2/CeS-NiCo LDH/NF and e) Ni_3S_2/Bi_2S_3-NiCo LDH/NF at the different scan rates varying from 20 to 100 mV·s^{-1}.

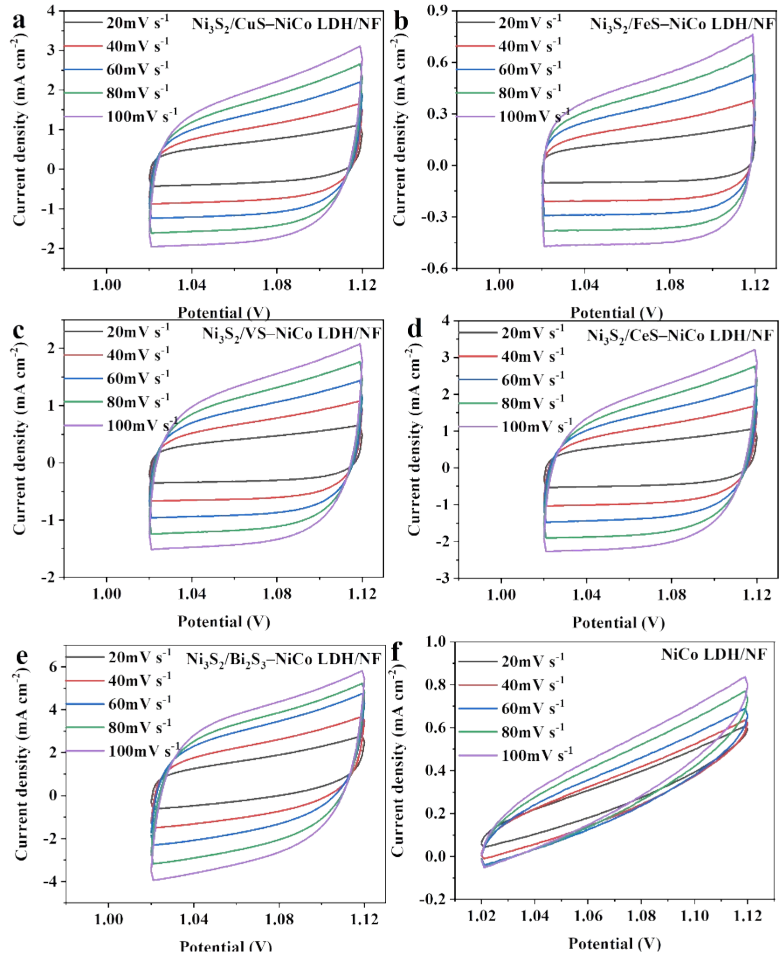

Fig. S11 In 1.0 M KOH with 0.5 M urea, UOR cyclic voltammograms of a) Ni_3S_2/CuS-NiCo LDH/NF, b) Ni_3S_2/FeS-NiCo LDH/NF, c) Ni_3S_2/VS-NiCo LDH/NF d) Ni_3S_2/CeS-NiCo LDH/NF and e) Ni_3S_2/Bi_2S_3-NiCo LDH/NF at the different scan rates varying from 20 to 100 $mV \cdot s^{-1}$.

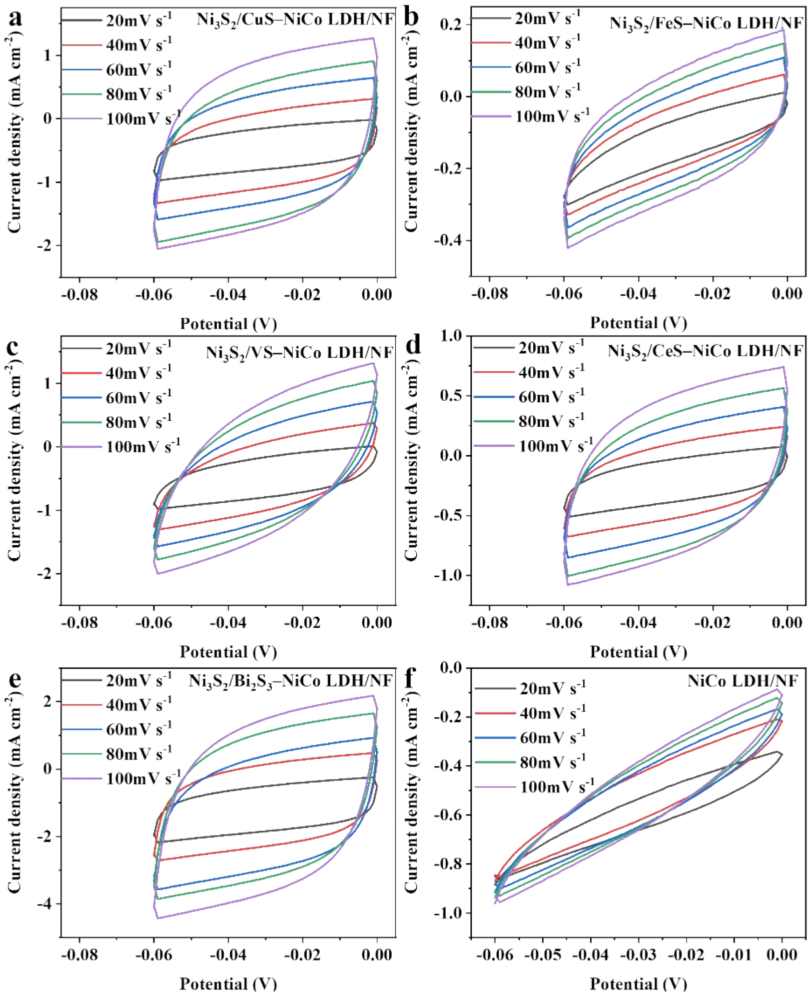

Fig. S12 In 1.0 M KOH with 0.5 M urea, HER cyclic voltammograms of a) Ni_3S_2/CuS-NiCo LDH/NF, b) Ni_3S_2/FeS-NiCo LDH/NF, c) Ni_3S_2/VS-NiCo LDH/NF d) Ni_3S_2/CeS-NiCo LDH/NF and e) Ni_3S_2/Bi_2S_3-NiCo LDH/NF at the different scan rates varying from 20 to 100 mV·s^{-1}.

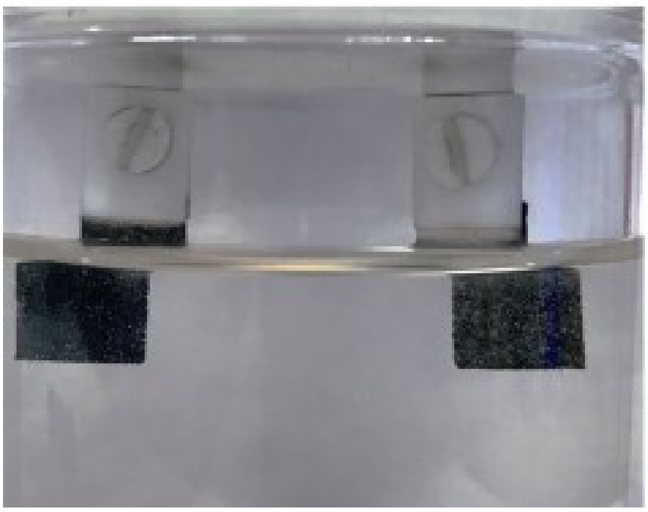

Fig. S13 The physical image of H_2 and O_2.

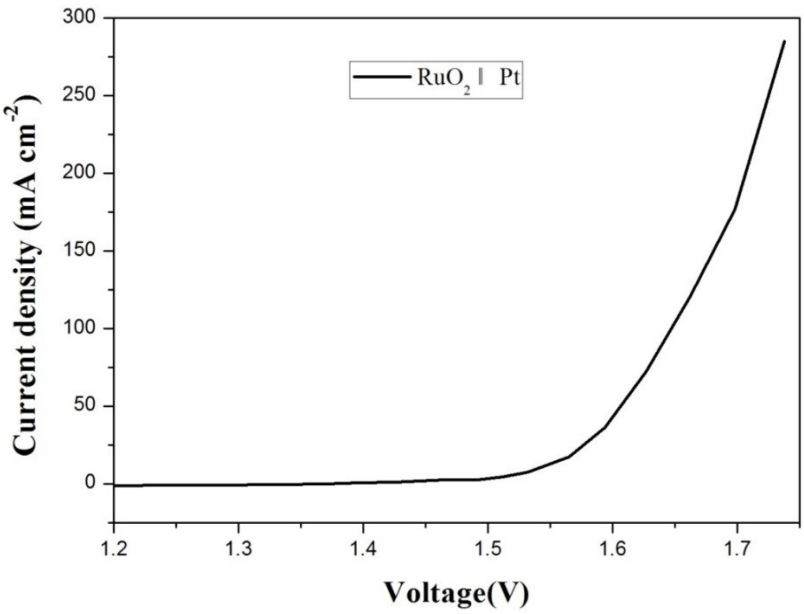

Fig. S14 Polarization curve of the RuO_2 and Pt for water splitting with a scan rate of 5 mV s^{-1} in 1 M KOH.

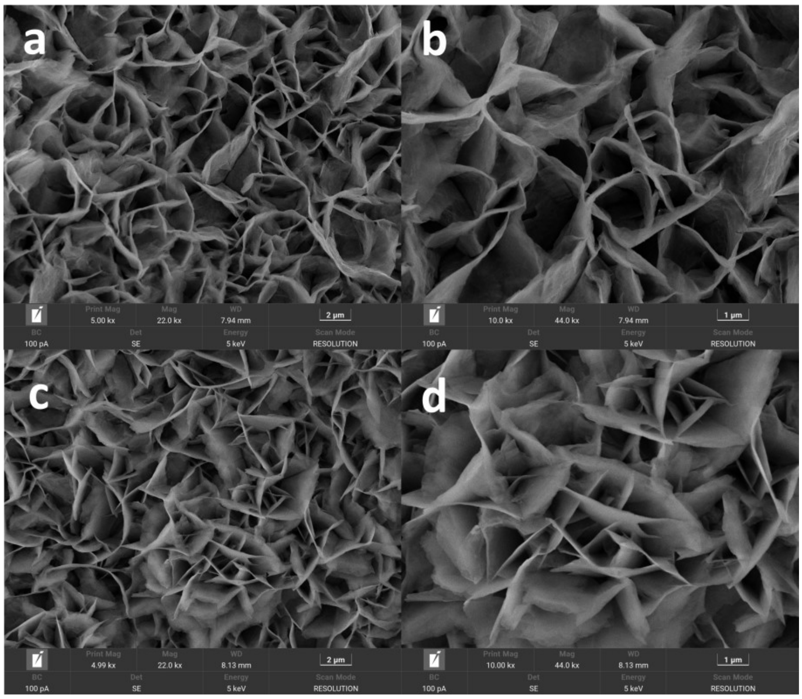

Fig. S15 SEM of Ni_3S_2/Bi_2S_3-NiCo LDH/NF after 12 h for (a-b) OER and (c-d) UOR.

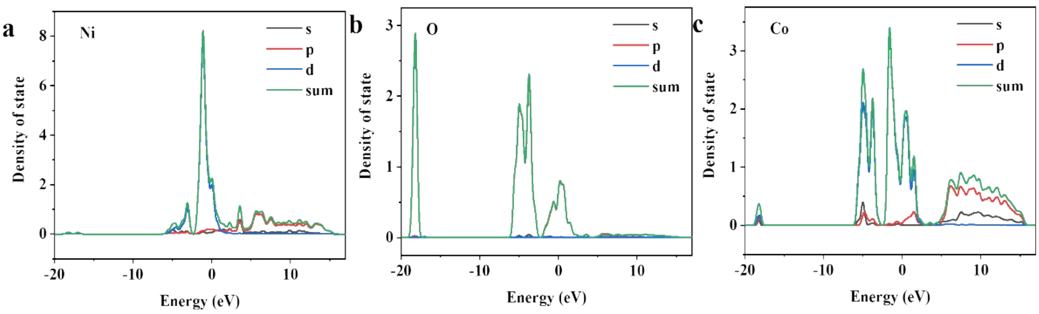

Fig.S16 Density of states for the Co-Ni$(OH)_2$, (a) Ni, (b) O and (c) Co.

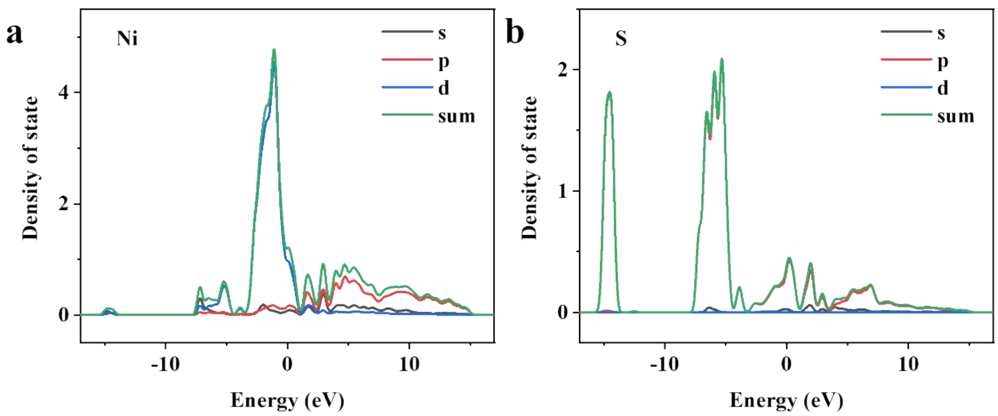

Fig.S17 Density of states for the Ni_3S_2, (a) Ni and (b) S.

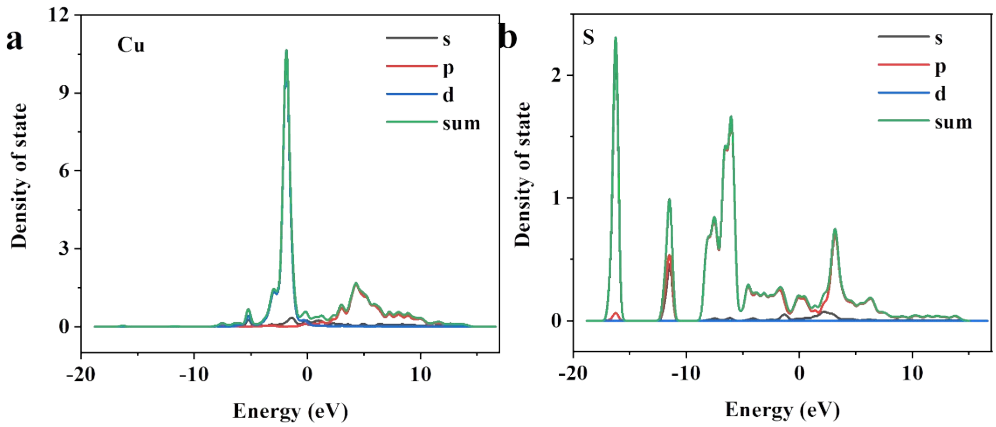

Fig.S18 Density of states for the CuS, (a) Cu and (b) S.

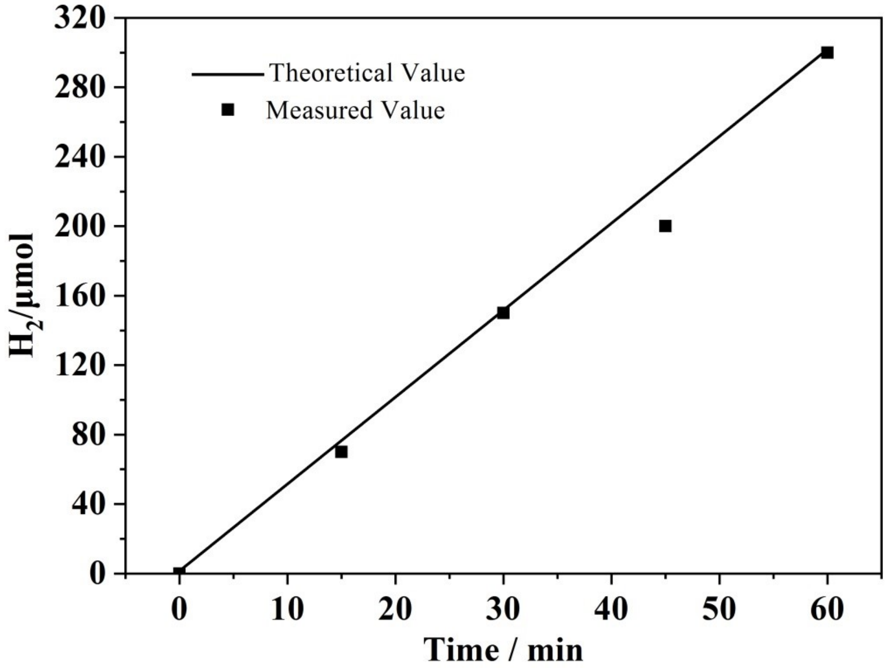

Fig. S19 Electrocatalytic efficiency of H_2 production over Ni_3S_2/Bi_2S_3-NiCo LDH/NF.

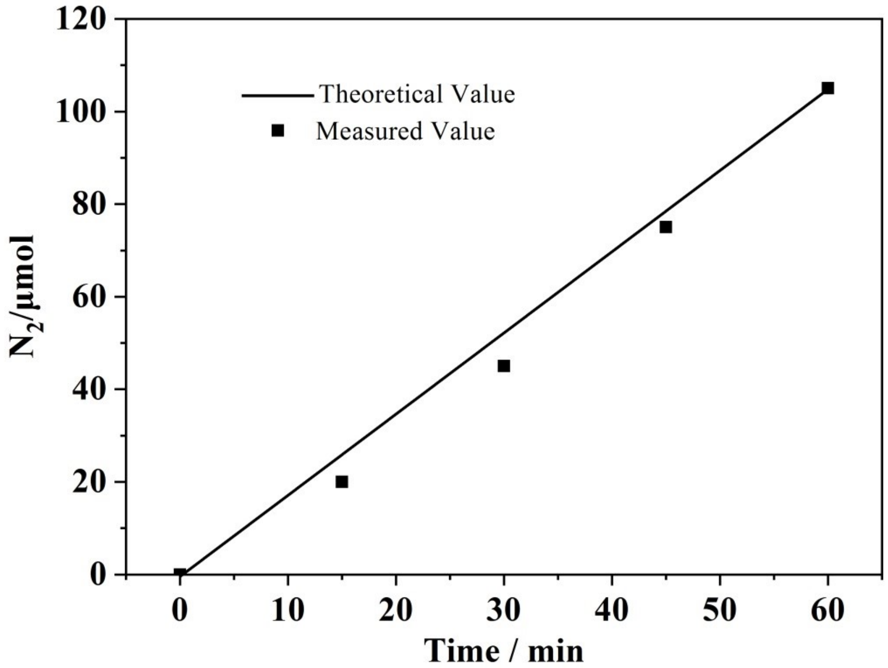

Fig. S20 Electrocatalytic efficiency of N_2 production over Ni_3S_2/Bi_2S_3-NiCo LDH/NF.

Supplementary Table

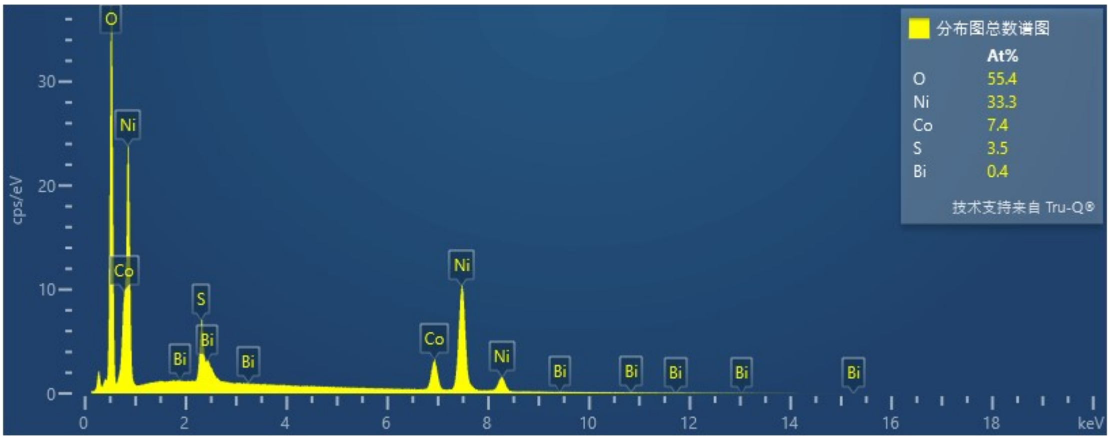

Element	Mass fraction %	Atomic fraction %
Co	4.34	5.8
Ni	13.22	20.91
O	63.38	51.32
S	2.55	2.66
Bi	0.13	0.12
C	16.38	19.19

[1] H.J. Zhang, X.P. Li, A. Hahnel, V. Naumann, C. Lin, S. Azimi, S.L. Schweizer, A.W. Maijenburg, R.B. Wehrspohn, Bifunctional Heterostructure Assembly of NiFe LDH Nanosheets on NiCoP Nanowires for Highly Efficient and Stable Overall Water Splitting;Adv. Funct. Mater., 2018;28.

[2] J.M. Huo, Y. Wang, L.T. Yan, Y.Y. Xue, S.N. Li, M.C. Hu, Y.C. Jiang, Q.G. Zhai, In situsemi-transformation from heterometallic MOFs to Fe-Ni LDH/MOF hierarchical architectures for boosted oxygen evolution reaction;Nanoscale, 2020;12: 14514-23.

[3] F.F. Yuan, Z.H. Liu, G.X. Qin, Y.H. Ni, Fe-Doped Co-Mo-S microtube: a highly efficient bifunctional electrocatalyst for overall water splitting in alkaline solution;Dalton Transactions, 2020;49: 15009-22.

[4] R. Zhang, R.L. Zhu, Y. Li, Z. Hui, Y.Y. Song, Y.L. Cheng, J.J. Lu, CoP and Ni2P implanted in a hollow porous N-doped carbon polyhedron for pH universal hydrogen evolution reaction and alkaline overall water splitting;Nanoscale, 2020;12: 23851-8.

[5] H. Zhao, M. Jiang, Q. Kang, L.Q. Liu, N. Zhang, P.C. Wang, F.M. Zhou, Electrocatalytic oxygen and hydrogen evolution reactions at Ni3B/Fe2O3 nanotube arrays under visible light radiation;Catal. Sci. Technol., 2020;10: 8305-13.

[6] F.C. Wu, G. Ou, J. Yang, H.N. Li, Y.X. Gao, F.M. Chen, Y. Wang, Y.M. Shi, Bifunctional nickel oxide-based nanosheets for highly efficient overall urea splitting;Chem. Commun., 2019;55: 6555-8.

[7] L. Yan, Y.L. Sun, E.L. Hu, J.Q. Ning, Y.J. Zhong, Z.Y. Zhang, Y. Hu, Facile in-situ growth of Ni2P/Fe2P nanohybrids on Ni foam for highly efficient urea electrolysis;J.Colloid.Interf .Sci., 2019;541: 279-86.

[8] C.Y. Zhang, T.T. Chen, H. Zhang, Z.H. Li, J.C. Hao, Hydrated-Metal-Halide-Based Deep-Eutectic-Solvent-Mediated NiFe Layered Double Hydroxide: An Excellent Electrocatalyst for Urea Electrolysis and Water Splitting;Chem-Asian. J., 2019;14: 2995-3002.

[9] H.Z. Xu, K. Ye, K. Zhu, J.L. Yin, J. Yan, G.L. Wang, D.X. Cao, Template-directed assembly of urchin-like CoSx/Co-MOF as an efficient bifunctional electrocatalyst for overall water and urea electrolysis;Inorg. Chem. Front., 2020;7: 2602-10.

[10] Q. Li, W.X. Zhang, J. Shen, X.Y. Zhang, Z. Liu, J.Q. Liu, Trimetallic nanoplate arrays of Ni-Fe-Mo sulfide on FeNi3 foam: A highly efficient and bifunctional electrocatalyst for overall water splitting;J.Alloy.Compd., 2022;902.